

**Calculated Dynamic Response and Loads  
for an Advanced Tip Rotor  
in Forward Flight**

**Philippe Benquet**  
Ministère de la Défense  
STPA, Département Hélicoptère  
Paris, FRANCE

and

**Inderjit Chopra**  
Center for Rotorcraft Education and Research  
Department of Aerospace Engineering  
University of Maryland  
College Park, Maryland 20742, USA

**FIFTEENTH EUROPEAN ROTORCRAFT FORUM**

SEPTEMBER 12 - 15, 1989 AMSTERDAM

# Calculated Dynamic Response and Loads for an Advanced Tip Rotor in Forward Flight

**Philippe Benquet**  
Ministère de la Défense  
STPA, Département Hélicoptère  
Paris, FRANCE

and

**Inderjit Chopra**  
Center for Rotorcraft Education and Research  
Department of Aerospace Engineering  
University of Maryland  
College Park, Maryland 20742, USA

## 1 ABSTRACT

The effect of tip sweep and droop on loads and response of a hingeless blade in forward flight are investigated. The blade as well as the tip are treated as elastic beams undergoing flap bending, lag bending, elastic twist and axial deflections. Geometric angles between blade and tip segments are retained before and after bending. An existing finite element comprehensive rotor dynamic code is modified consistently to incorporate new inertia, aerodynamic and structural forces caused by sweep and droop angles at blade tip. A finite element formulation based on Hamilton's principle is adopted and each element consists of fifteen degrees of freedom. The vehicle trim and blade steady responses are calculated iteratively as one coupled solution using a modified Newton method. Parametric studies of tip sweep and droop are carried out on a four-bladed soft-inplane hingeless rotor. Tip sweep has a powerful influence on the torsional dynamic behavior of the blade, due to the pitch-flap coupling. A small aft-sweep angle of  $5^\circ$  reduces vibratory hub loads by 14% for vertical hub forces, 5% for longitudinal hub forces and 17% for lateral hub forces. Tip droop causes pitch-lag coupling and has a substantial effect on steady as well as vibratory hub loads.

## 2 INTRODUCTION

Vibration reduction devices, such as passive isolators, dynamic absorbers and active higher harmonic control systems are adopted as the primary means to control vibration in helicopters at this time. With the emerging refinements and understanding of dynamic analysis of rotor systems, it is becoming possible to design rotors which inherently produce low vibratory forces. Recently, there has been a growing interest in the analysis of rotors with advanced tips, which appear attractive to reduce vibrations and hub loads, improve performance and enhance stability limits. With the application of composite, the potential of advanced tips has further enhanced.

A few experimental investigations showed the beneficial effect of tip sweep. At ONERA, experimental and theoretical studies were performed [8,23] in order to examine performance of new tip shapes. The aerodynamic and acoustic characteristics of rotor were seen to improve with swept-tip blades, especially due to the reduced wave drag and the intensity of the transonic flow at a high speed condition. At the NASA Langley Research Center, model rotor tests were conducted in the Transonic Dynamic Wind Tunnel to understand the mechanism for reduced vibrations with tip sweep. Conventional torsional stiff and reduced stiffness Aeroelasticity Conformable Rotor (ACR) blades were tested with several tip configurations. Results showed reductions in vibratory loads and shaft power [25]. Blackwell [10] showed that with a swept tip, advancing tip downloads can be used to produce a nose-up torsional moment which alleviates the tendency for nose-down twisting and tip-down bending of the advancing blade. Tip sweep acts as a feed-back mechanism to minimize fluctuations in oscillatory tip flatwise loading and thereby reduces vibration. He also pointed out that measured data on a CH-53D with several tips confirmed a tendency for lower airframe vibration when swept tips were used. The mechanism responsible for the reduced vibration were not clear from the test data.

One concern is the structural modeling of advanced tips. Recently, there have been some selected attempts to analyse dynamics of swept-tip rotors. Tarzanin and Vlaminc [21] conducted an analytical study to investigate the effect of blade sweep on vibratory loads including blade and control loads. The Boeing Vertol's aeroelastic rotor analysis program, C-60, was used. The 4/rev hub loads and rotor power were reduced by the use of blade tip sweep. The effect of sweep was introduced through an approximative modeling. The authors recommended the development of an improved analytical modeling for the swept-tip blades. Young, Tarzanin and Kunz [11] analysed a simplified model where the blade spanwise properties were reduced to constant values. Again, substantial vibratory hub loads were reduced with blade tip sweep. An extensive parametric study was conducted on the simplified model to determine which of the blade properties influence the 4/rev vertical hub loads the most. It was determined that the blade properties which were related to the dynamic torsional response of the blade were most important in determining the effectiveness of both aft and forward tip sweep. The authors postulated the sweep effect as an effective shift in cg-ac offset with respect to the unswept portion of the

blade. Two effects were identified which act on the blade to reduce the vibratory air loads due to tip sweep. These effects were :

- advancing blade untwist,
- favorable higher harmonic elastic pitch

that reduces the 4/rev airloads only. The structural modeling of swept tip was very approximate and therefore the results had to be viewed with caution.

Recently, Celi and Friedmann [1] developed an improved finite element formulation to analyse the stability and responses of hingeless rotor with swept tips in forward flight. The blade was modeled using the Galerkin finite element technique and a special element for the structural, inertial and aerodynamic properties of the swept tip was developed. Angle between inboard blade and tip segments was held fixed before and after bending, and transfer function for the swept tip was derived for linear deflections. However, the inertial matrices for the tip were derived consistently for moderate rotations retaining non-linear terms up to second order. It was shown that the tip sweep introduces flap-torsion and lag-axial couplings, which may lead to aeroelastic instability associated with frequency coalescence. A comparison with an equivalent sweep model using a straight elastic axis and offsets of aerodynamic centers and center of gravity (frequently adopted by other researchers) with their more exact swept tip model showed considerable discrepancy for a hingeless rotor. This raised questions to the values of conclusions arrived by other researchers. The optimization process developed by the authors showed that the introduction of tip sweep can reduce the n/rev vertical hub shears beyond the level that can be obtained by just modifying the mass and stiffness distributions of the blade. On the whole, the tip sweep showed a powerful influence on the dynamic behavior of a rotor blade.

Recently, Panda [13] derived the more exact constraint relations required during assembly of two moderate rotation finite elements joined together at an angle. The constraint relations were derived for a generic case of fixed sweep, droop and prepitch angles as well as variable angles introduced at hinges. The transformation matrix was obtained consistently for non-linear deflections and one cannot always neglect them by use of linear transformations.

From the overview of the past research works related to advanced tip rotors, it appears that the effect of tip droop, or anhedral on rotor dynamics is not investigated in any depth. Also, in light of precise transformation relations derived by Panda, it is important to examine the effect of tip sweep and droop on blade dynamics in a consistent manner.

### **3 OBJECTIVES**

The objective of this research is to investigate the effects of tip sweep as well as tip droop on loads and responses of a rotor system in forward flight. For this purpose, the existing comprehensive rotor dynamic finite element code developed in house at the University of Maryland has been modified to include the effects of tip

sweep and droop in a consistent manner. Siverani and Chopra [5] made a finite element formulation based on Hamilton's principle to investigate aeroelastic stability of elastic, articulated and hingeless blades in hover. Later on, Siverani and Chopra [2] extended their finite element formulation in hover for bearingless rotor blades.

Panda and Chopra [6] formulated stability of hingeless and bearingless rotor blades in forward flight. To model blade structural characteristics, the finite element formulation of [2] was used. Steady rotor response in forward flight was calculated using a quasilinear procedure, based on Floquet theory. Panda and Chopra [15] adopted a finite element in time procedure to calculate steady response in forward flight for hingeless composite blades. Recently, Lim and Chopra [14] improved the analysis to calculate the rotor coupled trim and response solutions in forward flight. This rotor dynamic analysis consists of two phases :

- vehicle trim and rotor steady response
- aeroelastic stability of the blade.

The vehicle trim solution determines the control settings and vehicle attitude for the prescribed flight condition. The steady response involves the determination of time dependent blade deflections at different azimuth positions for a time period of one complete cycle using a finite element method in time, which is based on Hamilton's weak principle. The vehicle trim and blade steady response were calculated iteratively as one coupled solution using a modified Newton method. The blade stability was calculated from perturbation equation using Floquet transition matrix theory.

This basic analysis is extended here to include the effects of tip sweep and droop in a generic way. The specific objectives of this research are :

- To modify the finite element formulation to incorporate the effects of sweep and droop at the tip in a consistent manner;
- To conduct parametric studies to investigate the effects of blade tip sweep and droop on a four-bladed soft-inplane hingeless rotor.

## **4 FORMULATION OF HAMILTON'S PRINCIPLE**

The analysis is made for an isolated rotor with elastic blades and advanced tips. Each blade as well as tip are assumed to be elastic beams undergoing flap bending, lag bending, elastic twist and axial deflections. The formulation is developed for nonuniform blade having pretwist, precone and chordwise offsets of center of gravity and aerodynamic center from the elastic axis. The aerodynamic loads are obtained based on a quasisteady strip theory approximation. The flow is assumed to be incompressible and inviscid.

The finite element formulation is based on Hamilton's principle

$$\delta \pi = \int_{t_1}^{t_2} (\delta U - \delta T - \delta W) dt = 0$$

where  $\delta U$ ,  $\delta T$  and  $\delta W$  are the variations of strain energy, kinetic energy and virtual work done by external forces. Substituting suitable expressions for  $\delta U$ ,  $\delta T$  and  $\delta W$  in Hamilton's principle results in equations of motion.

#### 4.1 Blade Geometry and Elastic Axis

The addition of a swept and drooped tip to the original straight blade implies the creation of new undeformed and deformed frames to modelize the outer tip part. Torsion will be considerably affected by sweep and droop, and, therefore, has to be carefully defined (cf [0]).

The elastic axis of the blade is defined as the locus of the shear centers of the cross section of the blade. Therefore, the elastic axis of the straight portion of the blade coincides with the pitch axis of the blade. A shear force applied at a point on the elastic axis of the straight portion will not produce torsional deformation.

The elastic axis of the swept tip is the line of shear centers of the cross sections outboard of the junction with the straight portion, and forms an angle with the inboard elastic axis. In general, a shear force applied at a point on the elastic axis of the swept tip will produce torsional deformation in the whole blade.

The two elastic axis are continuous at the junction.

A point on the elastic axis of the straight portion of the blade undergoes two geometric rotations in the undeformed blade frame (a pretwist due to and a cyclic and collective input) and an elastic twist in the blade deformed frame. The geometric twist calculated in the deformed blade frame differs from the geometric twist calculated in the blade undeformed frame by a second order term only.

A point on the elastic axis of the tip undergoes geometric rotations and translations operated in the undeformed blade and tip frames (due to the geometric rotations at the junction point and the pretwist of the tip element) and an elastic twist operated in the tip deformed frame. In the calculation of the total pitch angle wrt the deformed tip frame, sweep and droop angles at the junction point affect linearly the pretwist angle expressed in the deformed tip frame.

#### 4.2 Strain Energy

Considering the uniaxial stress assumption, which is valid for a long, slender beam such as rotor blades, the expression for the variation of strain energy in term of the classical strains is

$$\delta U = \int_0^R \iint_A (E \epsilon_{xx} \delta \epsilon_{xx} + G \epsilon_{x\eta} \delta \epsilon_{x\eta} + G \epsilon_{x\xi} \delta \epsilon_{x\xi}) d\eta d\xi dx$$

The explicit expressions for strains are described in [2] and are unchanged by the present research. The expression for the variation of strain energy in a nondimensional form is obtained retaining up to second order terms, which are important for the axial and torsion equations.

### 4.3 Kinetic Energy and Inertial Loads

These are calculated in the undeformed tip coordinate system. During the calculation of the derivatives of an arbitrary point on the swept tip with respect to time, a lot of linear terms appear as the contribution of the conjugation of sweep and droop angles with elastic deformations of the tip. The kinetic energy variations can be written in a nondimensional manner retaining terms up to second order as :

$$\frac{\delta T}{m_0 \Omega^2 R^3} = \int_0^1 (\bar{z}_u \delta u + \bar{z}_v \delta v + \bar{z}_w \delta w + \bar{z}_\phi \delta \phi + \bar{z}_{v'} \delta v' + \bar{z}_{w'} \delta w') dx$$

Inertial forces and moments at an arbitrary spanwise location on the rotor swept tip are calculated in a similar manner, and used in the calculations of blades loads.

### 4.4 Virtual Works and Aerodynamic Loads

The quasisteady strip theory approximation is used. The linear inflow model is adopted from Drees. The circulatory aerodynamic loads obtained in the deformed tip frame are expressed in the undeformed tip frame using transformation matrix. The noncirculatory aerodynamic loads about the elastic axis in the undeformed tip frame are obtained from the thin airfoil theory.

The virtual work  $\delta W$  done by external forces may be defined as

$$\delta W = \int_0^1 (L_u^A \delta u + L_v^A \delta v + L_w^A \delta w + M_u^A \delta \phi) dx$$

where the L are the aerodynamic forces distributed along the tip length in the axial, lead-lag and flap direction, and M is a twisting moment about the undeformed elastic axis.

## 4.5 Finite Element Method in Space

The variation of total virtual energy can be expressed in terms of elastic deflections  $u$ ,  $v$ ,  $w$  and  $\phi$  by substitution. Applying finite element method in space for this virtual energy expression would result in finite element equation of motion.

The blade and the tip are discretized into a number of beam elements. Each beam element consists of fifteen degrees of freedom. There are two internal nodes for an axial deflection and one internal node for an elastic twist. Between elements, there is a continuity of displacement and slope for lag and flap bending deflection and a continuity of displacement for elastic twist and axial deflections. The swept tip is discretized by one fifteen degrees of freedom element. At the junction, the assembly requires special attention [13], as shown in § 4.6. For lag and flap bending deflections, interpolating functions are chosen from Hermite family polynomials, which may allow a continuity of displacement and slope. For elastic twist and axial deflections, Lagrange family polynomials are used, since they may give a continuity of displacement. At the junction node, the 6 nodal displacements are expressed in the undeformed blade coordinate system, while the other nodal displacements of the swept tip are kept in the undeformed tip coordinate system (figure ). Therefore, the junction node response will be the typical blade response in terms of lag, flap, axial and torsion deflections, while the other tip external nodes will be typical swept tip responses expressed in its own undeformed coordinate system.

The virtual energy can be written in terms of the nodal displacement quantities in the space domain :

$$\Delta_j = \delta q_j^T (M_j \ddot{q}_j + C_j \dot{q}_j + K_j q_j - F_j)$$

where  $M_j$ ,  $C_j$ ,  $K_j$  and  $F_j$  are elemental mass, damping, stiffness and load matrices respectively. Assembling these elemental matrices with the technique detailed in § 4.6, gives the nonlinear equations of motion in terms of nodal displacements. In the assembled matrices, boundary conditions are enforced. This gives finite element equations of motion as follows :

$$M\ddot{q} + C\dot{q} + Kq = F$$

## 4.6 Assembly of Two Moderate Rotation Finite Element Joined at Fixed Angles

The relations derived by Panda [13] are applied here at the junction of the blade with the advanced tip. The two moderate rotation finite elements are joined at fixed angles, namely sweep and droop. Therefore, the constraint relations between the element rotational degrees of freedom of the interconnected nodes are nonlinear. For linear case only, the conventional linear transformation is valid. Figure 7 shows the assembly of the two elements adjoining, labeled as 1 and 2. The element degrees of freedom are described with respect to its undeformed local element

frame. The assembly of the translation degrees of freedom [u,v,w] is straightforward through a geometrical transformation matrix :

$$\begin{Bmatrix} u_2 \\ v_2 \\ w_2 \end{Bmatrix} = T_{\Lambda} \begin{Bmatrix} u_1 \\ v_1 \\ w_1 \end{Bmatrix}$$

where  $T_{\Lambda}$  is defined in [0]. The assembly of the rotational degrees of freedom [ $\theta, w', v'$ ] yields three nonlinear constraint relations between the left and right element rotational degrees of freedom, as given in [0] :

$$\begin{Bmatrix} \theta_2 \\ w'_2 \\ v'_2 \end{Bmatrix} = (T_{\Lambda}^* + T_{\Lambda R}^K) \begin{Bmatrix} \theta_1 \\ w'_1 \\ v'_1 \end{Bmatrix} = T_{\Lambda R} \begin{Bmatrix} \theta_1 \\ w'_1 \\ v'_1 \end{Bmatrix}$$

For velocity and acceleration, the constraint relations are :

$$\begin{Bmatrix} \dot{\theta}_2 \\ \dot{w}'_2 \\ \dot{v}'_2 \end{Bmatrix} = (T_{\Lambda}^* + T_{\Lambda R}^C) \begin{Bmatrix} \dot{\theta}_1 \\ \dot{w}'_1 \\ \dot{v}'_1 \end{Bmatrix}$$

$$\begin{Bmatrix} \ddot{\theta}_2 \\ \ddot{w}'_2 \\ \ddot{v}'_2 \end{Bmatrix} = (T_{\Lambda}^* + T_{\Lambda R}^C) \begin{Bmatrix} \ddot{\theta}_1 \\ \ddot{w}'_1 \\ \ddot{v}'_1 \end{Bmatrix} + T_{\Lambda R}^M \begin{Bmatrix} \dot{\theta}_1 \\ \dot{w}'_1 \\ \dot{v}'_1 \end{Bmatrix}$$

All  $T_{\Lambda R}$  matrices depend linearly on elastic deformations  $u, v, w, \theta, v', w', \theta, w', v'...$

## 5 COUPLED TRIM ANALYSIS

The coupled trim analysis in forward flight consists of three major phases : vehicle trim, blade steady response and hub loads calculation. For vehicle trim, the propulsive trim analysis is used. The blade steady response is calculated using finite element method in time. Hub loads are calculated using force summation

method. In the existing rotor dynamic analysis code, a complete coupled solution involving all three phases has been calculated iteratively, using a modified Newton method, as shown in [14].

The vehicle trim analysis existing in the existing dynamic code is not changed for the purpose of the present research. A summary of the analysis is given here but more details can be seen in [14], or in [0].

### **5.1 Vehicle Trim Analysis**

To start the procedure, a simple propulsive trim analysis is made based on the flap dynamics of a rigid blade. This analysis determines the control settings and vehicle attitude for the prescribed flight conditions. The trim solution is calculated from the overall nonlinear vehicle equilibrium equations : three force equations and two moment equations. The yawing angle of the fuselage is assumed to be aligned along the longitudinal hub axis. For an approximation of the nonuniform inflow distribution at the rotor in forward flight, a linear variation of inflow over the rotor disk is used from Drees inflow modeling. The coupled equations obtained can be solved iteratively by nonlinear system equation solver routine.

### **5.2 Blade Steady Response (Finite Element Method in Time)**

The blade steady response solution involves the determination of time dependent blade deflections at different azimuth locations, using finite element method in time. Description of finite element method in time is available in [9], [14] and [15]. A brief description is given here.

The time period of one rotor revolution is discretized into a number of time elements (typically 6 to 10). To reduce computation time, the space domain is transformed into the modal domain using the coupled natural vibration modes of the blade (obtained from the homogeneous undamped finite element equations in vacuum). The state vector is expressed in terms of normal coordinates, which are expressed in terms of nodal displacements and shape functions, for the corresponding time element. Interpolating fourth-order polynomials are taken from Lagrangian polynomial family. The finite element in time formulation is based on Hamilton's weak principle.

Resulting normal mode equations are ultimately solved as a set of non-linear algebraic equations. The solution is obtained utilizing an iterative, modified Newton method. The steady response is determine iteratively until a converged solution is achieved.

### **5.3 Hub Loads Calculation**

The calculation of steady hub loads are required to trim the helicopter. The higher harmonic components are responsible for the helicopter vibration but has a negligible influence on vehicle trim solution.

The hub loads include six components of hub forces and moments in the nonrotating hub-fixed frame, such as longitudinal ( $F_x$ ), lateral ( $F_y$ ) and vertical

( $F_z$ ) hub shear forces, and rolling ( $M_x$ ), pitching ( $M_y$ ) and yawing ( $M_z$ ) hub moments. These hub loads are obtained from the summation of blade loads.

The blade loads include six components of blade root forces and moments, radial ( $F_x$ ), drag ( $F_y$ ) and vertical ( $F_z$ ) shear forces, and the torsional ( $M_x$ ), flapwise ( $M_y$ ) and lagwise ( $M_z$ ) moments in the undeformed blade frame.

For a helicopter vibration reduction purpose, one needs to calculate the harmonics of the blade root and hub loads. For a 4-bladed rotor, 3/rev and 5/rev in plane root shear forces (radial and drag), 4/rev vertical root shear force, 3/rev and 5/rev torsional and flapwise root moments, and 4/rev lagwise root moment are transmitted to the hub as primary sources of helicopter vibration. Therefore, 3/rev, 4/rev and 5/rev higher harmonics of hub loads are always involved in 4-bladed rotor vibration problems.

#### 5.4 Procedure of Coupled Trim Analysis

The coupled trim analysis determines vehicle trim parameters iteratively from the satisfaction of overall vehicle equilibrium equations. These equilibrium equations show inherent couplings between a rotor and fuselage of a helicopter, which make the analysis more complex. Hence, the blade steady response, hub loads and overall vehicle equilibrium equations are solved simultaneously.

## 6 RESULTS AND DISCUSSION

Results are obtained for a four-bladed soft-inplane hingeless rotor with Lock number  $\gamma = 5$ , thrust level  $C_t/\sigma = 0.07$ , solidity ratio  $\sigma = 0.07$ , zero precone and advance ratio  $\mu = 0.35$ . The static airfoil characteristics are

$$C_l = 2\pi\alpha$$

$$C_d = 0.01 + 0.2\alpha^2$$

$$C_m = 0.$$

Blade properties are assumed uniform in the spanwise direction and are given in table 1. For the baseline configuration (no sweep and no droop), the fundamental frequencies are : flap frequency of 1.126/rev, lag frequency of 0.7/rev and torsion frequency of 4.47/rev. The blade is discretized into 5 elements of equal length. The outboard element is set at different sweep ( $\Lambda_1$ ) and droop ( $\Lambda_2$ ) angles, ranging from  $+10^\circ$  to  $-40^\circ$ . This means that the sweep or droop angles are given only to the outer 20% of the blade length.

### 6.1 Effects of sweep

Figure 9 presents the effects of tip sweep on fundamental rotating frequencies. With an increasing sweep angle, there is a slight increase of the first torsion frequency and a slight decrease of the second torsion and second axial

frequencies. There is only slight influence of sweep on other modes. The centrifugal force stiffens the torsion mode of the blade due to the tennis racket effect. Tip sweep increases this action by offsetting the tip center of gravity from the blade elastic axis. Therefore, the blade becomes stiff in torsion and the first torsion frequency increases.

Figures 10, 11 and 12 present the flap, lag and torsion deflections at the tip. These deflections are nondimensionalized with respect to the rotor radius and expressed in the reference frame of the tip. A *negative sweep represents an aft-swept tip* (opposite to rotation) whereas a *positive sweep represents a forward-swept tip*. An aft sweep increases the peak-to-peak flapping amplitude and a forward sweep decreases it. The mean flapping amplitude however decreases with an increasing aft-sweep. There is a considerable effect of tip sweep on mean amplitude of lag response. For a forward tip sweep, the lagging amplitude increases (larger lag angle) whereas for an aft tip sweep, the blade deflects more forward (larger lead-lag angle). This is due to the kinematic axial-lag coupling and the straightening effect of the centrifugal force. An aft tip sweep induces a larger nose-up tip twist whereas a forward tip sweep causes a nose-down twist at the tip. This elastic twist is defined about the tip axis and is the result of three different factors :

- a component of flap angle at the junction,
- a twisting of blade due to shift of tip aerodynamic center,
- a twisting due to centrifugal force caused by flap angle.

Therefore, due to kinematic coupling at the junction, axial-lag and flap-torsion modes, the tip deflections are very dependent on blade deflections. Sometimes, these kinematic couplings work contrary to the direct aerodynamic/inertial couplings.

Figures 13, 14 and 15 present the flap, lag and torsion deflections at the junction between blade and tip, in the undeformed reference frame of the blade. The flap and lag deflections are quite similar to those at the tip. However, there is a considerable difference in elastic twist at the tip and at the junction. An aft-sweep angle of less than  $10^\circ$  induces a nose-down twist, which is quite opposite than the twist observed at the tip. This can be explained from the fact that kinematic coupling caused by flap angle at the tip does not occur at the junction. For a larger aft-sweep angle (more than  $10^\circ$ ), this trend changes and a nose-up twist occurs at the junction. Actually, the aft-swept tip undergoes two opposite loads : an upload due to aerodynamic forces and a down load due to inertia forces (figure 6). Uploads and downloads at the swept tip are transmitted respectively as nose-down and nose-up twist at the junction by the kinematic flap-torsion coupling. For low aft sweep angle, the aerodynamic load is more predominant and induces a nose-down twist at the junction. For a larger aft sweep angle, the aerodynamic load decreases with the tip angle of attack, whereas the download due to centrifugal force increases and thus induces a nose-up twist at the junction.

Figures 16, 17 and 18 respectively show radial shear  $F_x$ , chordwise shear  $F_y$  and vertical root shear  $F_z$  for one complete cycle. There is only a small influence of tip sweep on these shear forces.

Figure 19 present flap moment at blade root. It consists primarily of 2/rev harmonic, and its amplitude increases with a larger aft sweep of tip. A forward tip sweep reduces flap moment (10% reduction for a  $10^\circ$  forward sweep).

Figure 20 shows lag moment at blade root. It consists primarily of a 1/rev variation and there is only a small change in amplitude with tip sweep. It is interesting to note that the general variations of flap and lag moments are quite similar to those of flap and lag deflections (Figures 13 and 14).

Figure 21 presents torsional moment at blade root. There is a substantial change in torsional moment with tip sweep. The variation of torsional moment appears identical to the variation of elastic twist at the blade junction (figure 15). It consists primarily of a 3/rev harmonic and a phase shift of 180° occurs between aft-sweep to forward-sweep configurations.

The hub forces and moments are transmitted to the airframe and are the primary source of vibrations. Figure 22, 23 and 24 respectively show longitudinal, lateral and vertical hub forces. For a 4-bladed rotor, one expects primarily 4/rev hub forces in the fixed reference frame. There is change in oscillatory and steady amplitudes with tip sweep. Also, the phase of 4/rev harmonic changes with sweep. The change in steady amplitude of longitudinal and lateral forces reflects the new trim attitude  $\Phi_s$  and  $\alpha_s$  reached by the airframe (table 2). A large sweep angle, both forward and aft, increases oscillatory amplitudes of hub forces. With the changing sweep angle, the steady component of vertical hub force is unaffected since the rotor thrust is held fixed. It is interesting to note that the minimum oscillatory hub forces occur for a small aft sweep angle (say 5°).

Figures 25, 26 and 27 respectively show rolling, pitching and yawing hub moments. There is a change in the oscillatory amplitudes with tip sweep. Also, the yawing moment steady amplitude is reduced by an aft-sweep, caused by the stiffening effect of the centrifugal force. The steady components of roll and pitch hub moments remain unaffected because of trim constraints. Again, the phase of 4/rev harmonics change from aft sweep to forward sweep of tip.

Figures 28 and 29 respectively show the variations of peak-to-peak oscillatory amplitudes of hub forces and moments with tip sweep. A minimum of hub forces occurs for an aft sweep angle of 5° whereas there is no well defined minimum for hub moments. Comparing oscillatory hub forces for an aft sweep of 5° with unswept blade, the vertical hub force amplitude is reduced by 14%, the longitudinal hub force amplitude is reduced by 5% and the lateral hub force amplitude is reduced by 17%.

## 6.2 Effects of Droop

Droop represents an initial flap setting for the tip segment; a *positive droop* represents upward flap angle and a *negative droop* represents downward flap angle. Droop is given to the outer 20% of blade length.

Figure 30 presents the effects of tip droop on fundamental rotating frequencies. There is an increase of the first torsion frequency and a decrease of the *second lag frequency*, which in fact becomes 4/rev for a droop of 12°. There are only slight effects of droop on others modes.

Figures 31, 32 and 33 respectively represent the flap, lag and torsion deflections at the tip, presented in the undeformed reference frame of the tip. There is a considerable effect of tip droop on mean amplitude of flap response. For a downward tip droop, it increases. This phenomenon is similar in nature to the change in lag response for a blade with tip sweep, and is due to the straightening effect of the centrifugal force. A droop angle increases the lagging amplitude. Lag deflection at the tip consists primarily of a 1/rev variation harmonic except for a droop of  $-10^\circ$  where it becomes a 4/rev component. It corresponds to a droop angle for which the rotating second lag frequency becomes equal to 4/rev. A phase shift can also be observed in the 1/rev harmonic when droop angle changes from negative to positive value. Torsion deflection at the tip consists primarily of a 4/rev harmonic except for the baseline configuration (no droop) where it is a 1/rev amplitude. The oscillatory amplitude is maximum for a droop angle of  $-10^\circ$ . Also, there is a large phase shift between droop angles of  $-10^\circ$  and  $-20^\circ$ , may be attributed to the occurrence of resonance condition of second lag mode with 4/rev for tip droop of  $-10^\circ$ . The elastic twist is the result of two different factors :

- a component of lag angle at the junction,
- a twisting of the blade.

The lag angle at the junction includes a weak nose-up twist for a negative droop angle due to the kinematic lag-torsion coupling (figure 8), and results in nose-down twist for a positive droop angle. Therefore, like a swept-tip blade, the tip deflections are dependent on inboard blade deflections, induced by the kinematic axial-flap and lag-torsion couplings.

Figures 34, 35 and 36 present respectively the flap, lag and torsion deflection at the junction between blade and tip, in the undeformed reference frame of the blade. The flap and lag deflections are quite similar to those at the tip. Comparing with lag deflection variation at tip (Figure 32), the lag deflection at the junction does not contain the 4/rev component for a droop angle of  $-10^\circ$ . The steady elastic twist amplitude is not affected by droop, a big contrast to the elastic twist distribution at tip. The variations observed at the tip are caused by the kinematic lag-torsion coupling which is absent for the inboard section. The oscillatory amplitude of the 4/rev harmonic of twist at the junction increases substantially for a droop angle of  $-10^\circ$  and shows the possibility of resonance of 4/rev with low damped second lag mode.

Figures 37, 38 and 39 respectively show radial shear  $F_x$ , chordwise shear  $F_y$  and vertical shear  $F_z$  for one complete cycle. There is a negligible influence of droop on radial shear force. Chordwise shear  $F_y$  shows a large 4/rev harmonic for a droop angle of  $-10^\circ$  similar to the lag deflection variation at tip. The amplitude of the vertical shear is reduced by a down-droop (25% of reduction for a droop angle of  $-20^\circ$ ) and a large 3/rev harmonic appears for a droop angle of  $-10^\circ$ .

Figures 40, 41 and 42 respectively show the flap, lag and torsion moments at blade root. A down-droop reduces the oscillatory amplitude of flap moment (15% for a droop angle of  $-20^\circ$ ) which consists primarily of a 2/rev harmonic. The lag moment shows a 1/rev component for the straight blade, which becomes predominantly a 4/rev harmonic for a droop angle of  $-10^\circ$  (similar to the root chordwise shear force and the tip lag deflection variations). The torsion moment is

quite similar to the torsion deflection at blade junction, which consists of a 4/rev harmonic. A phase shift of  $180^\circ$  occurs between down-droop to up-droop configurations.

Figures 43, 44 and 45 respectively show longitudinal, lateral and vertical hub forces in the fixed reference frame. As expected, these variations primarily consist of 4/rev harmonics for the 4-bladed rotor. There is change in oscillatory as well as steady amplitudes with tip droop for the longitudinal and lateral forces. The changes in steady forces are due to new trim solutions  $\alpha_s$  and  $\Phi_s$  (table 3). The changes in oscillatory amplitude with droop angle are small. The hub steady vertical force does not change with droop, but its 4/rev harmonic shows a large amplitude for a droop angle of  $-10^\circ$ .

Figures 46, 47 and 48 respectively show rolling, pitching and yawing hub moments. Again, a large 4/rev amplitude and phase shift occur in the rolling and yawing moments for a droop angle of  $-10^\circ$ , due to the resonance condition of second lag mode with 4/rev forcing. The hub pitching moment is unaffected by droop and only shows a phase shift with droop angle.

Figures 49 and 50 respectively show the variations of peak-to-peak oscillatory amplitude of hub forces and hub moments with droop. The lateral hub force and rolling hub moment are reduced for a droop angle of  $-5^\circ$ . A droop angle of  $-10^\circ$  (down droop) leads to maximum amplitudes for all forces and moments, caused by the resonance of low damped second lag modes with the 4/rev harmonic.

## 7 CONCLUSIONS

This research investigated the influence of tip sweep and tip droop on the loads and response of a four-bladed soft-inplane hingeless rotor in forward flight. A finite element comprehensive rotor dynamic code has been modified consistently by assembling the outer tip element for arbitrary sweep and droop angles. Inertia, aerodynamic and structural operators with Hamilton's principle have been recalculated to account for the effects of sweep and droop. Based on the parametric study on a uniform hingeless rotor blade, the following conclusions are drawn :

### 7.1 Tip Sweep Effects

1. Tip sweep increases the first torsion fundamental frequency.
2. Tip aft sweep increases the oscillatory tip flap amplitude and has only a slight influence on mean tip flap amplitude. For lag response at tip, sweep has a negligible effect on oscillatory amplitude. Tip lags more with forward sweep. For elastic twist at tip, mean as well as oscillatory amplitudes are affected with sweep.
3. The torsion response at the junction consists of a nose-down twist for a small aft sweep angle and a nose-up twist for a larger aft sweep angle because of the predominance of centrifugal force.

4. Forward sweep reduces 4/rev flap moment. There is a considerable influence of sweep on torsion moment and its variation with sweep is quite identical to the elastic twist variation at junction.

5. Tip sweep changes steady amplitudes of longitudinal and lateral hub forces but the steady component of vertical hub force is unaffected. Tip sweep changes steady amplitude of yawing moment but the steady components of hub rolling and pitching moments are unaffected.

6. The minimum vibratory hub forces occur for a small aft sweep angle. For example, an aft sweep angle of  $5^\circ$  reduces the oscillatory amplitudes by 14% for vertical hub force, by 5% for longitudinal hub force and by 17% for lateral hub force.

## 7.2 Tip Droop Effects

1. Tip droop increases the first torsion fundamental frequency and decreases the second lag fundamental frequency, which in fact becomes 4/rev for a droop angle of  $12^\circ$  in our case.

2. Tip droop has a considerable influence on mean as well as oscillatory flap amplitude at tip. Tip droop has a slight influence on mean lag deflection at tip but the 1/rev oscillatory component becomes 4/rev for a droop angle of  $-10^\circ$ . For elastic twist at tip, any nonzero droop angle induces dominant 4/rev components which become large for a droop angle of  $-10^\circ$ .

3. Flap and lag responses at the blade junction are identical to those at the tip, except for the case of a  $-10^\circ$  droop angle in which the lag response remains essentially 1/rev. For elastic twist at junction, tip droop does not affect the mean amplitude but the 4/rev component increases substantially for a droop angle of  $-10^\circ$ . This is due to the resonance condition of low damped second lag mode with 4/rev forcing and a strong pitch-flap coupling.

4. There is only a small influence of the tip droop on mean amplitude of shears and moments at blade root, however oscillatory amplitude of shears and moments do change with droop setting. At droop angle of  $-10^\circ$ , the oscillatory amplitudes of shears and moments grow substantially due to the occurrence of resonance condition (second lag mode with 4/rev forcing).

5. Tip droop changes mean amplitude of hub longitudinal and lateral forces and yawing moment whereas the mean amplitude of hub vertical force, pitching and rolling moments are unaffected.

6. A tip droop of  $-10^\circ$  (down droop) leads to maximum peak-to-peak oscillatory amplitude for all forces and moments.

## REFERENCES

- [ 0 ] Ph. Benquet and I. Chopra, "Calculated Dynamic Response and Loads for an Advanced Tip Rotor in Forward Flight", M.S. Thesis, University of Maryland, 1988.
- [ 1 ] R. Celi, "Aeroelasticity and Structural Optimization of Helicopter Rotor Blades with Swept Tips", Ph.D. Dissertation, Mechanical, Aerospace and Nuclear Engineering Department, University of California, Los Angeles, October 1987.
- [ 2 ] N.T. Sivaneri and I. Chopra, "Finite Element Analysis for Bearingless Rotor Blade Aeroelasticity", Journal of the American Helicopter Society, April 1984.
- [ 3 ] D.H. Hodges, R.A. Ormiston and D.A. Peters, "On the Nonlinear Deformation Geometry of Euler-Bernoulli Beams", NASA TP-1566, April 1980.
- [ 4 ] D.H. Hodges and E.H. Dowell, "Nonlinear Equations of Motion for the Elastic Bending and Torsion of Twisted Nonuniform Rotor Blades", NASA, TN D-7818, December 1974.
- [ 5 ] N.T. Sivaneri and I. Chopra, "Dynamic Stability of a Rotor Blade Using Finite Element Analysis", AIAA Journal, May 1982.
- [ 6 ] B. Panda and I. Chopra, "Dynamic Stability of Hingeless and Bearingless Rotor Blades in Forward Flight", 1st International Conference on Rotorcraft Basic Research, Research Triangle Park, February 1985.
- [ 7 ] W. Johnson, "Recent Developments in the Dynamics of Advanced Rotor Systems", Vertica, Vol. 10, No. 1, 1986, pp 72-107 (part 1) and Vol. 10, No. 2, 1986, pp 109-150 (part 2).
- [ 8 ] J.J. Thibert and J.J. Philippe, "Etudes de profils et d'extrémités de pales d'hélicoptères", AGARD Conference Proceeding No. 334, May 1982, pp. 3-1/3-14.
- [ 9 ] J. Lim and I. Chopra, "Design Sensitivity Analysis for an Aeroelastic Optimization of a Helicopter Blade", SDM conference, Williamsburg, Virginia, April 1987.
- [ 10 ] R.H. Blackwell Jr, "Blade Design for Reduced Helicopter Vibrations", AHS Annual Forum, November 1981.
- [ 11 ] D.K. Young F.J. Tarzanin and D.L. Kunz, "Use of Blade Sweep to Reduce 4/rev Hub Loads", AHS Annual Forum, Saint-Louis, May 1987.

- [12] W.H. Weller, "Experimental Investigation of Effects of Blade Tip Geometry on Loads and Performance for an Articulated Rotor System", NASA TP, 1979.
- [13] B. Panda, "Assembly of Moderate Rotation Finite Element Used in Helicopter Rotor Dynamic", AHS Journal, TN, 1987.
- [14] J.W. Lim, "aeroelasticity Optimization of a Helicopter Rotor", Ph.D. Dissertation, University of Maryland, 1988.
- [15] B. Panda and I. Chopra, "Dynamics of Composite Rotor Blades in Forward Flight", A Special Issue to Mark Vertica's 10th Anniversary, Vertica, Vol 11, No. 1-2, 1986, pp 187-209.
- [16] P. Friedmann, "Recent Trends in Rotary-wing Aeroelasticity", Vertica, Vol. 11, No. 1, 1987, pp 139-170.
- [17] P. Friedmann, "Formulation and Solution of Rotary-Wing Aeroelasticity Stability and Response Problems", Vertica, Vol. 7, No. 2, 1983, pp 101-141.
- [18] R.A. Ormiston, "Investigation of Hingeless Rotor Stability", Vertica, Vol. 7, No. 2, pp 143-182.
- [19] F.K. Straub and P. Friedmann, "A Galerkin Type Finite Element Method for Rotary-Wing Aeroelasticity in Hover and Forward Flight", Vertica, Vol. 5, 1981, pp 75-98.
- [20] G.S. Bir and I. Chopra, "Gust Response of Hingeless Rotors", Journal of the AHS, Vol. 31, No. 2, April 1986, pp 36-46.
- [21] F.J. Tarzanin and R.R. Vlamincik, "Investigation of Blade Sweep on Rotor Vibratory Loads", NASA CR 166526, 1983.
- [22] M. Borri, "Helicopter Rotor Dynamics by Finite Element Time Approximation", Computer and Mathematical Application, Vol 12-A, 1986, pp 149-160.
- [23] A. Desopper, Ph. Lafon, P. Ceroni and J.J. Philippe, "10 Years of Rotor Flow Studies at ONERA - State of the Art and Future Studies", Proceedings of the 42th Annual Forum of the AHS, Washington D.C., June 1986, pp 267-277.
- [24] B. Monnerie and J.J. Philippe, "Aerodynamic Problems of Helicopter Blade Tips". 3rd European Rotorcraft and Powered-Lift Aircraft Forum, Vertica, Vol. 2, 1977, pp 217-231.
- [25] R.H. Blackwell, R.J. Murril, W.T. Yeager Jr. and P.H. Mirrick, "Wind Tunnel Evaluation of Aeroelastically Conformable Rotors", 1980.

[ 26 ] M.S. Torok and I. Chopra, "A Coupled Rotor Aeroelastic Analysis Utilizing Non-Linear Aerodynamics and Refined Wake Modelling", Proceeding of the Fourteenth European Rotorcraft Forum, No. 21, 1988.

TABLE I

Hingeless Blade Properties

$$\begin{aligned} EI_y/m_0 \Omega^2 R^4 &= 0.0108 \\ EI_z/m_0 \Omega^2 R^4 &= 0.0268 \\ GJ/m_0 \Omega^2 R^4 &= 0.00615 \\ EA/m_0 \Omega^2 R^4 &= 44.6 \\ e_g/c &= 0 \\ e_A/c &= 0 \\ e_d/c &= 0 \\ m/m_0 &= 1 \\ c/R &= 0.055 \end{aligned}$$

TABLE II

Trim Control Changes with Sweep Angle

$\Lambda_1$	$\alpha$	$\phi_s$	$\theta_0$	$\theta_{1c}$	$\theta_{1s}$
10	.1437	.0133	.1723	.0235	-.0971
0	.1473	.0159	.1744	.0307	-.0961
-10	.1520	.0179	.1788	.0357	-.0976
-20	.1581	.0171	.1859	.0393	-.1019

$$\mu = 0.35 \quad C_T/\sigma = 0.07$$

TABLE III

Trim Control Change with Droop Angle

$\Lambda_2$	$\alpha$	$\phi_s$	$\theta_0$	$\theta_{1c}$	$\theta_{1s}$
10	.1755	-.0292	.1705	.0526	-.0931
0	.1474	.0159	.1744	.0307	-.0961
-10	.1422	.0062	.1811	.0091	-.1044
-20	.1623	.0026	.1910	-.0115	-.1188

$$\mu = 0.35 \quad C_T/\sigma = 0.07$$

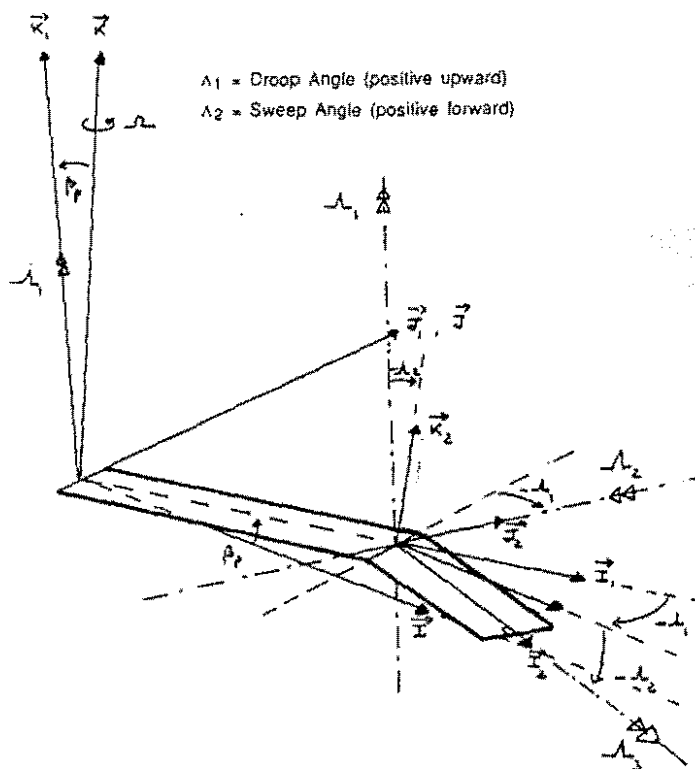


Figure 1

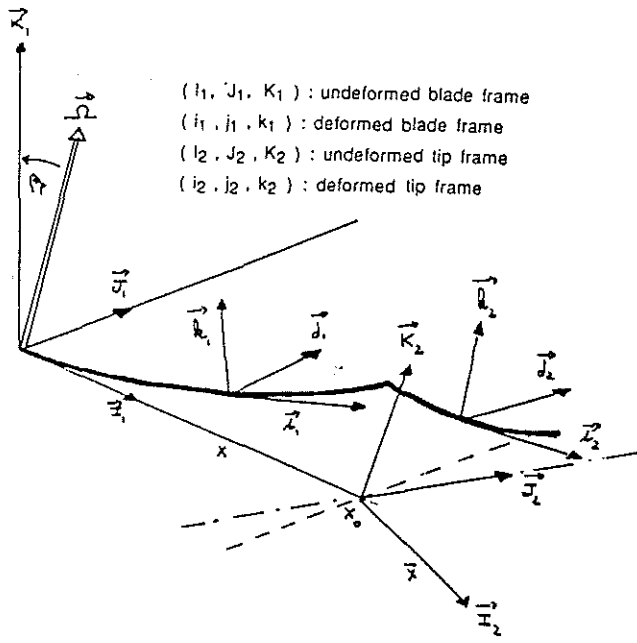


Figure 2

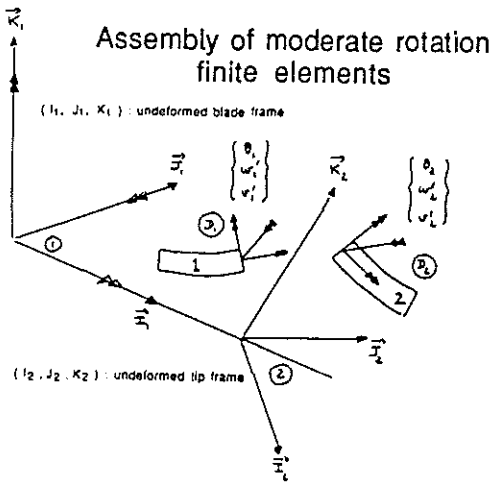


Figure 3

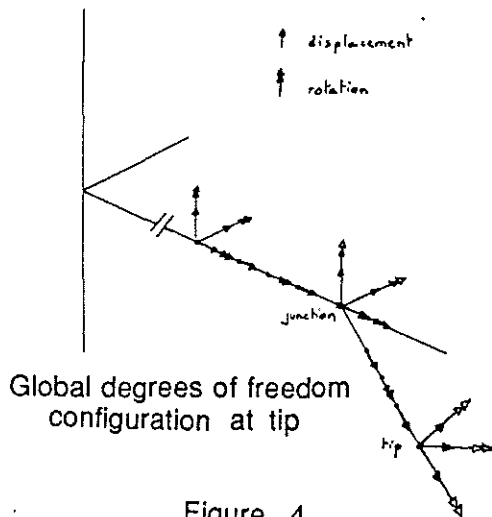


Figure 4

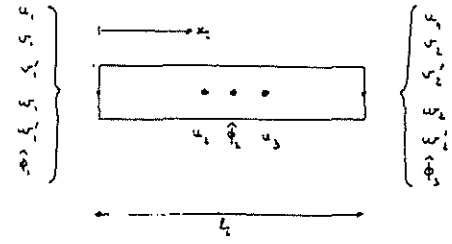


Figure 5

Aerodynamic and centrifugal forces on swept tip

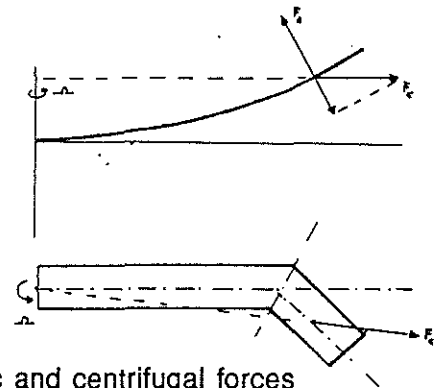


Figure 6

Pitch-flap coupling

for sweep angle

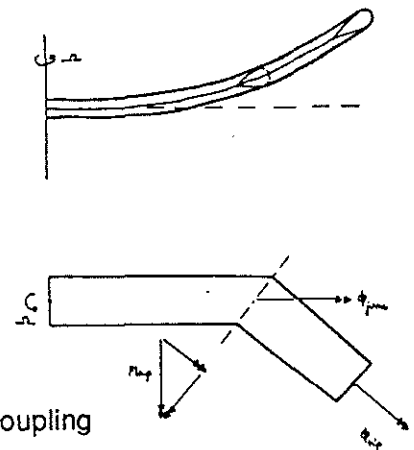


Figure 7

Pitch-lag coupling

for droop angle

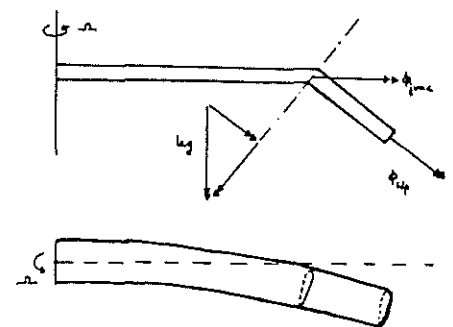


Figure 8

SWEEP AND FUNDAMENTAL FREQUENCIES

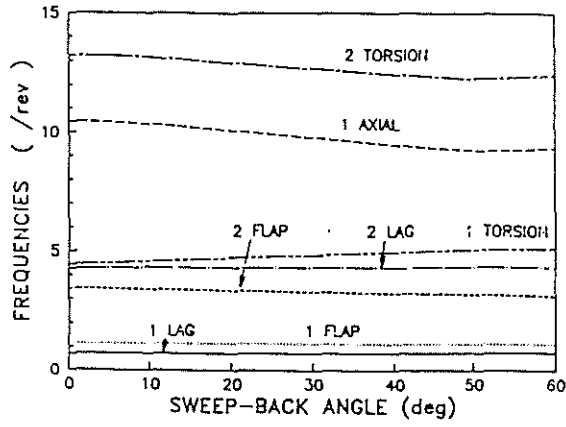


Figure 9

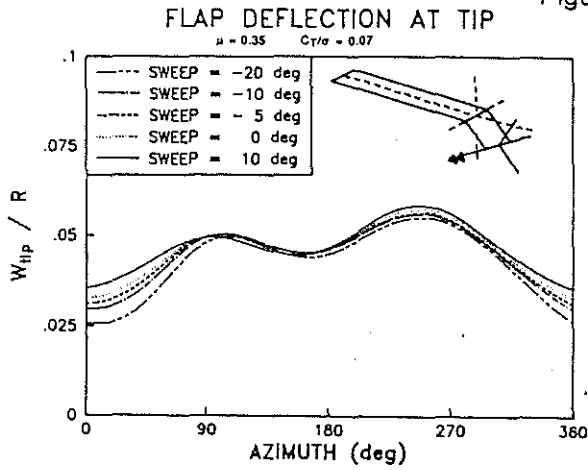


Figure 10

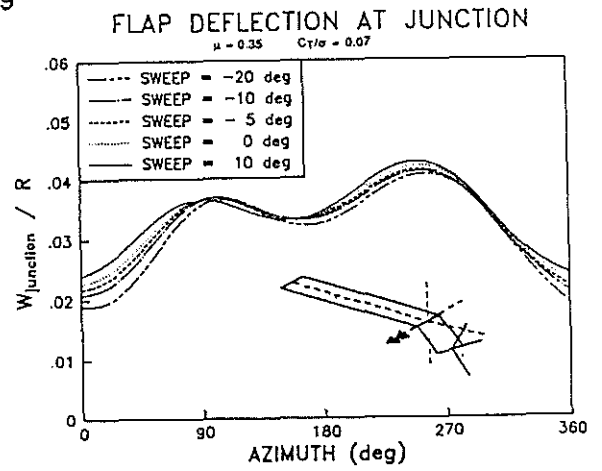


Figure 13

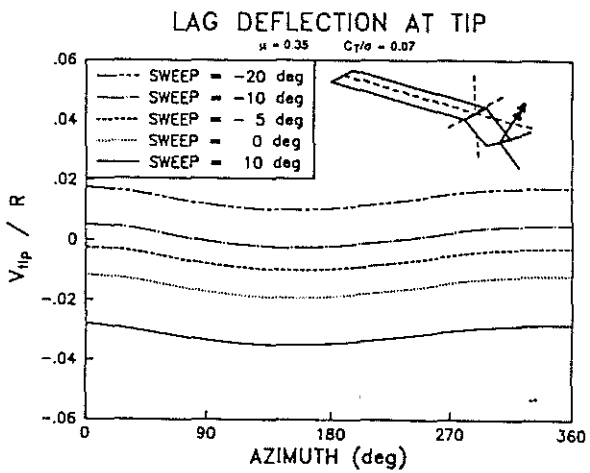


Figure 11

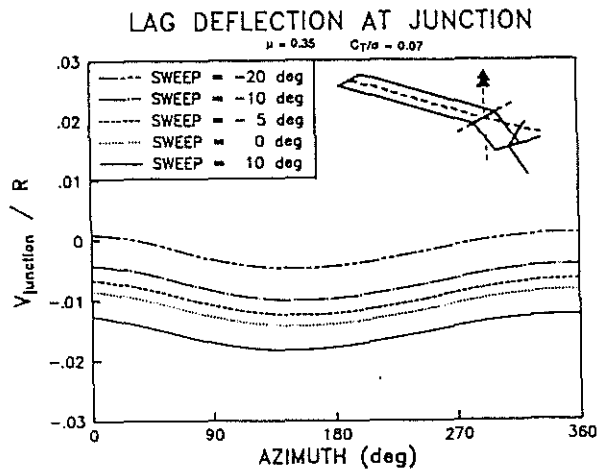


Figure 14

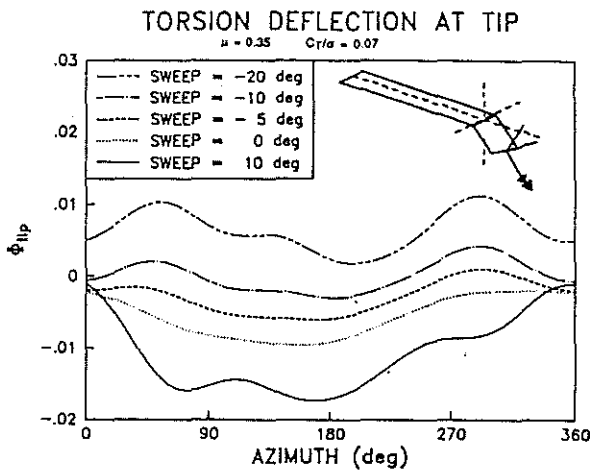


Figure 12

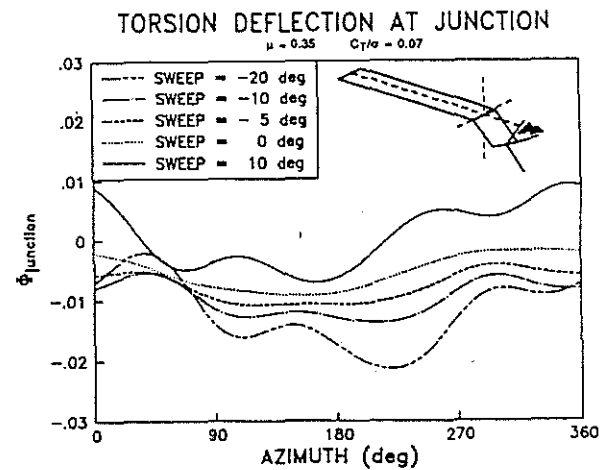


Figure 15

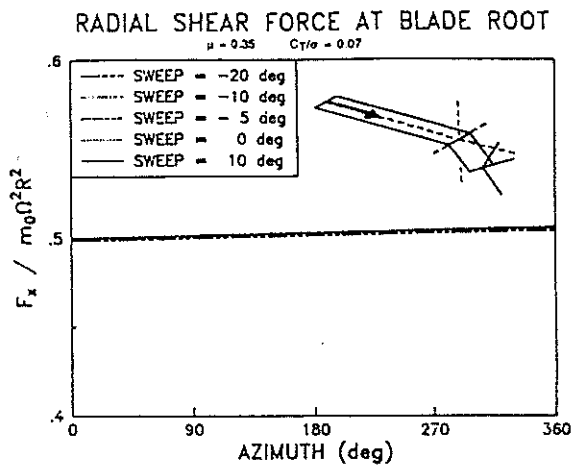


Figure 16

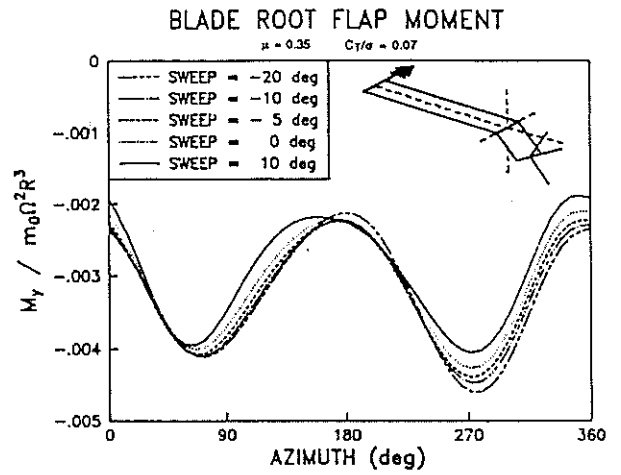


Figure 19

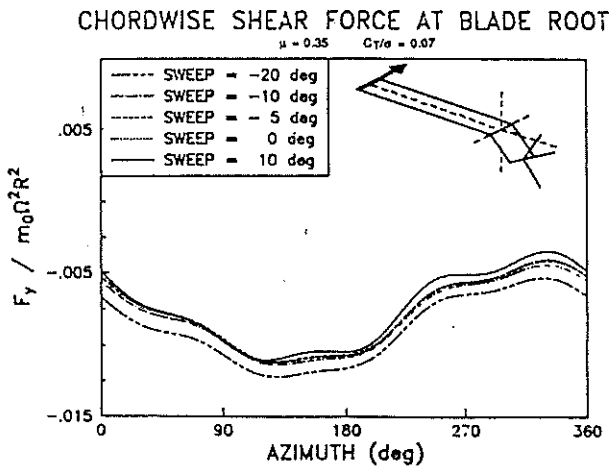


Figure 17

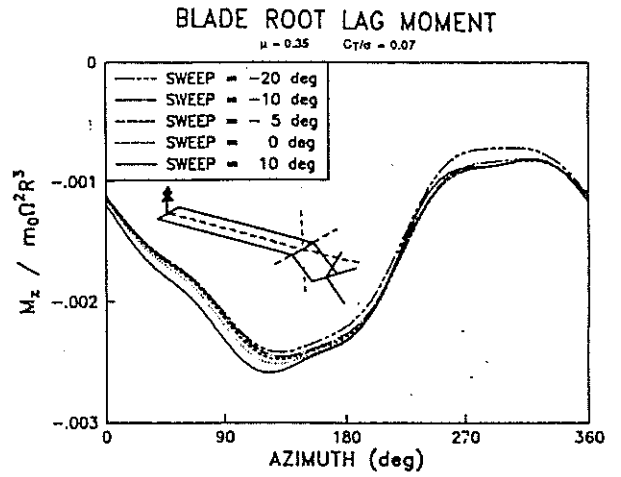


Figure 20

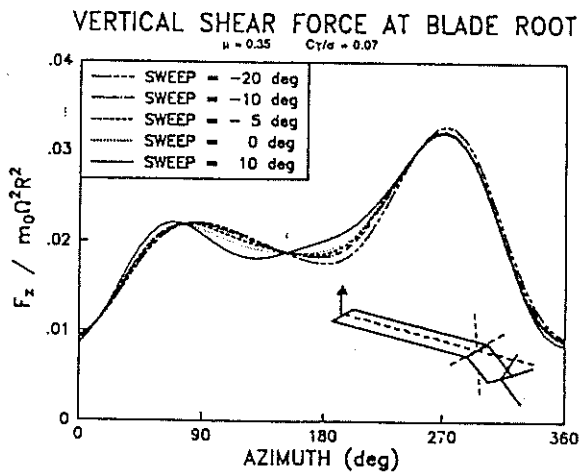


Figure 18

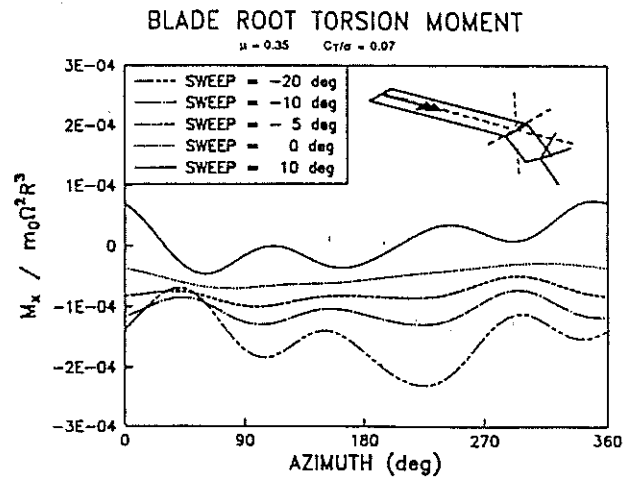
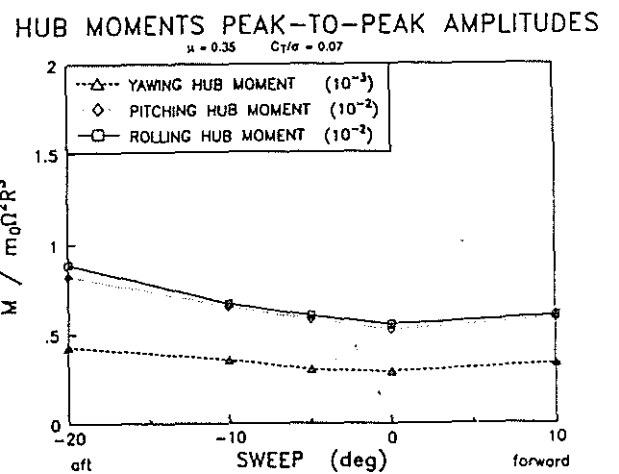
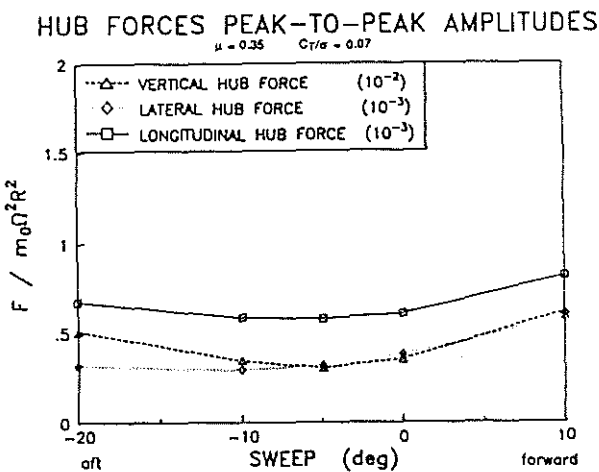
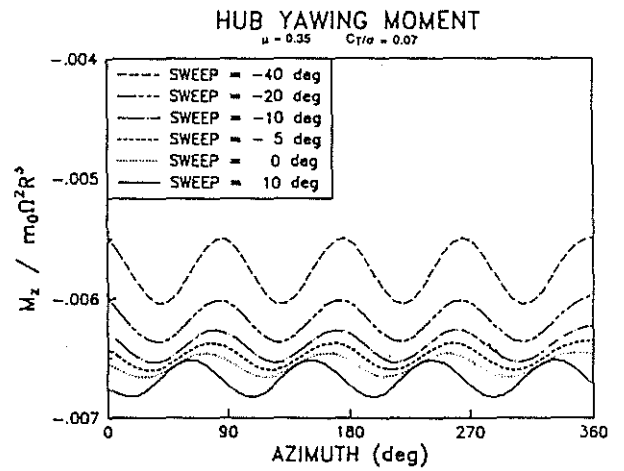
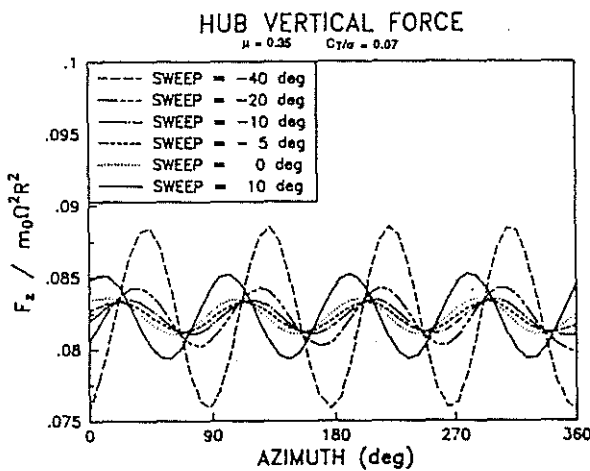
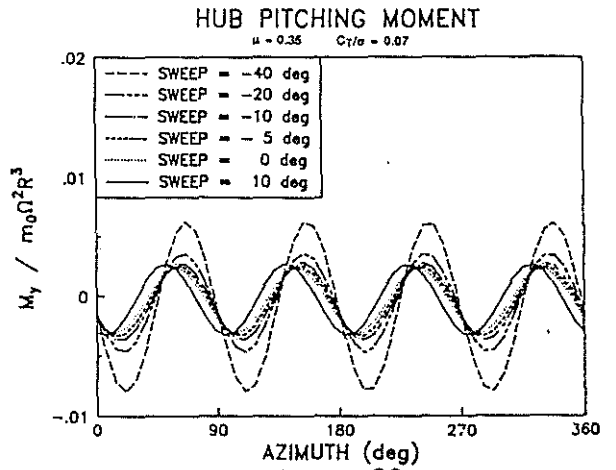
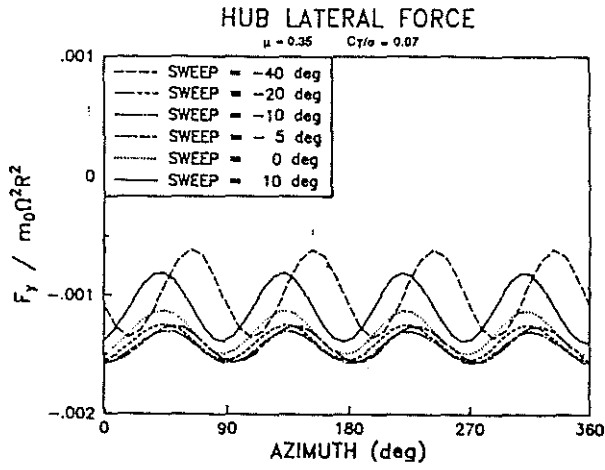
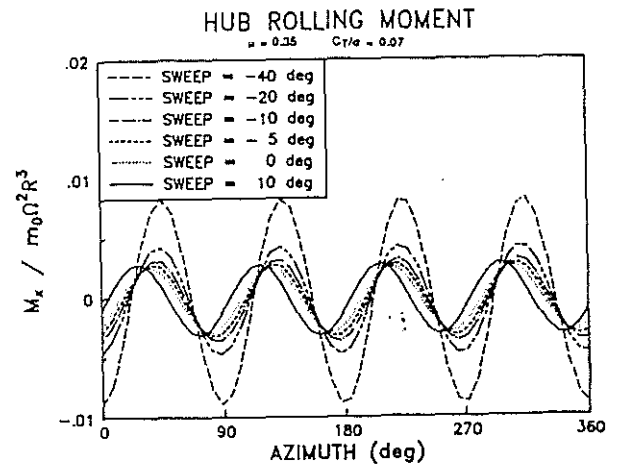
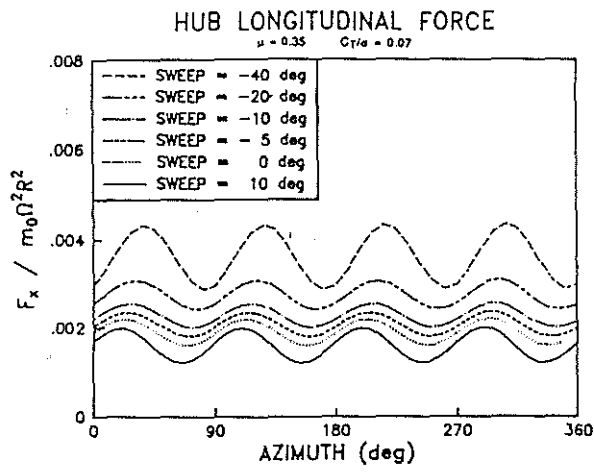


Figure 21



# DROOP AND FUNDAMENTAL FREQUENCIES

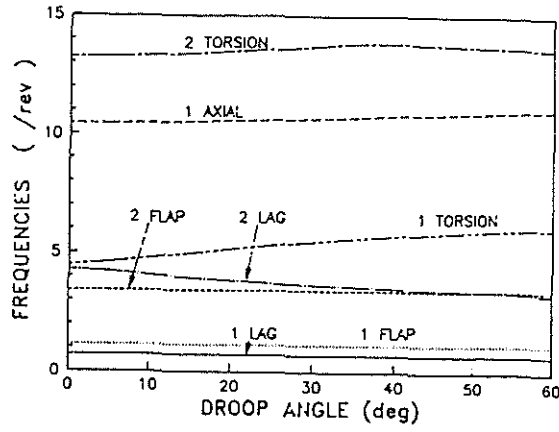


Figure 30

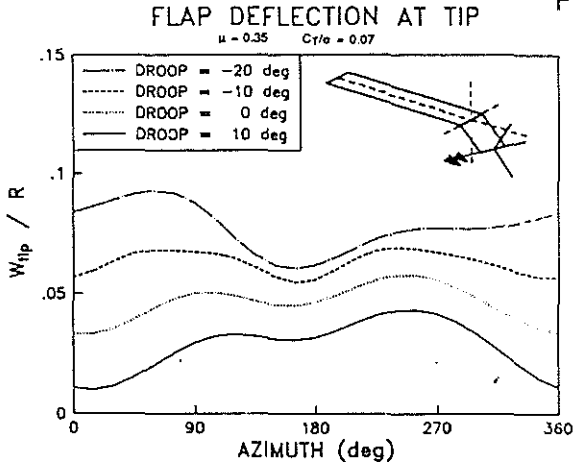


Figure 31

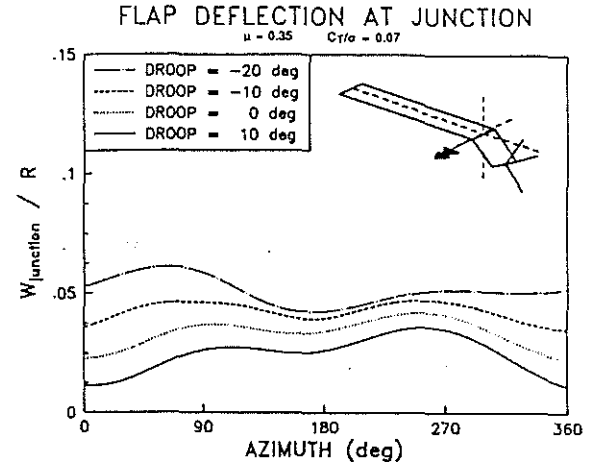


Figure 34

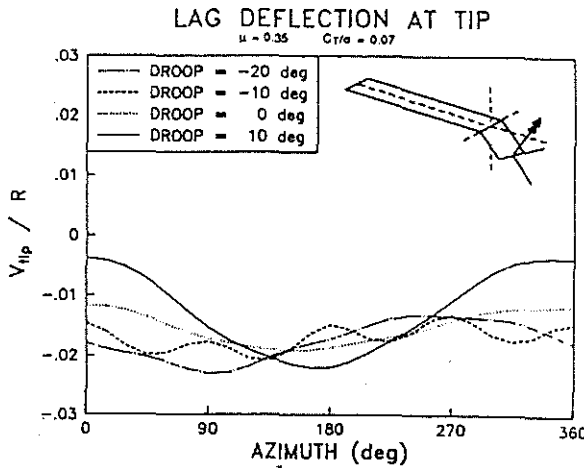


Figure 32

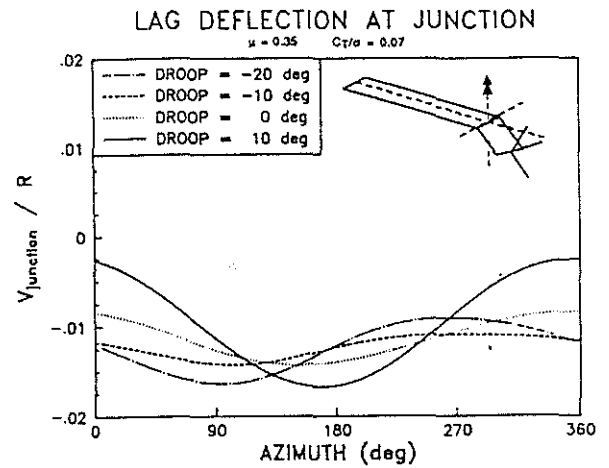


Figure 35

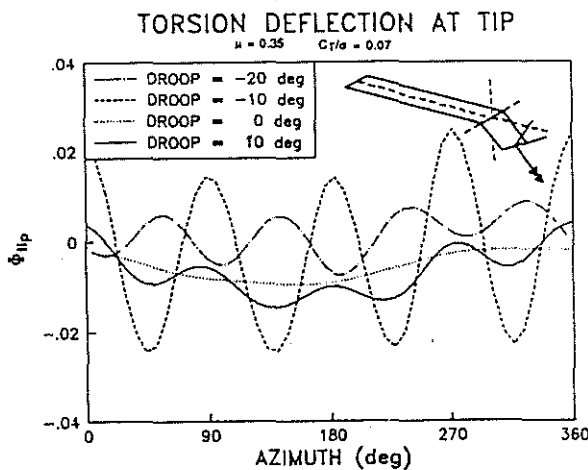


Figure 33

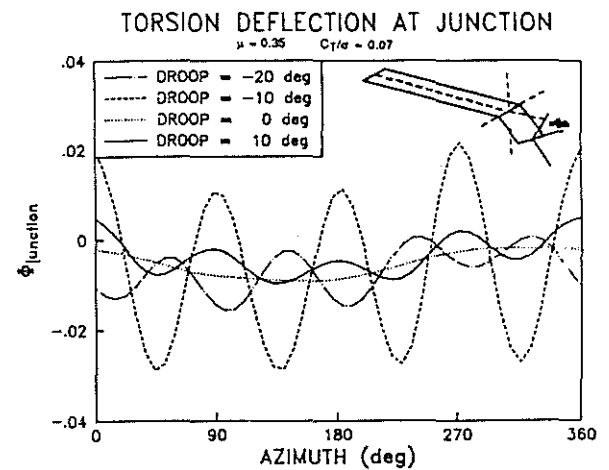
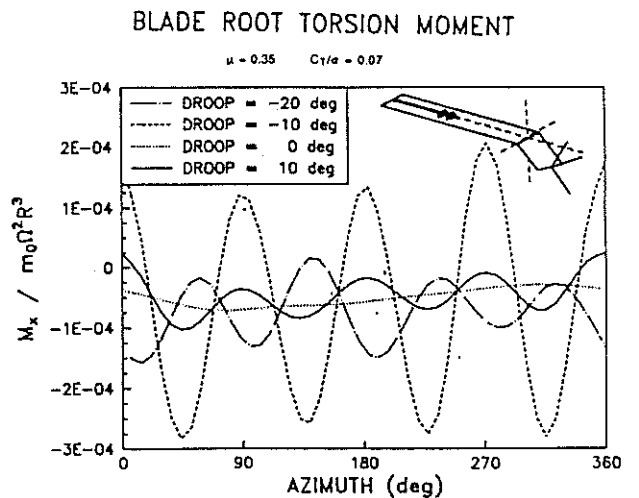
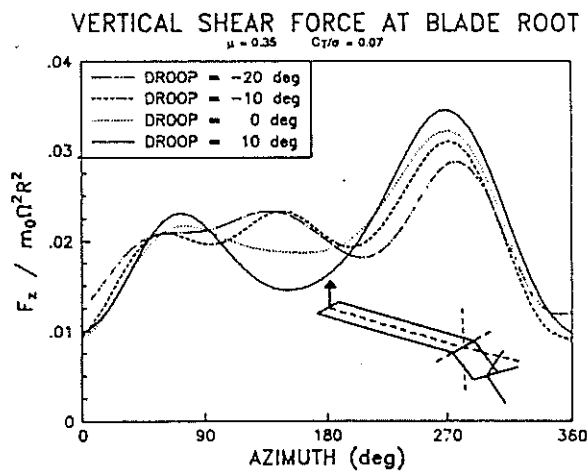
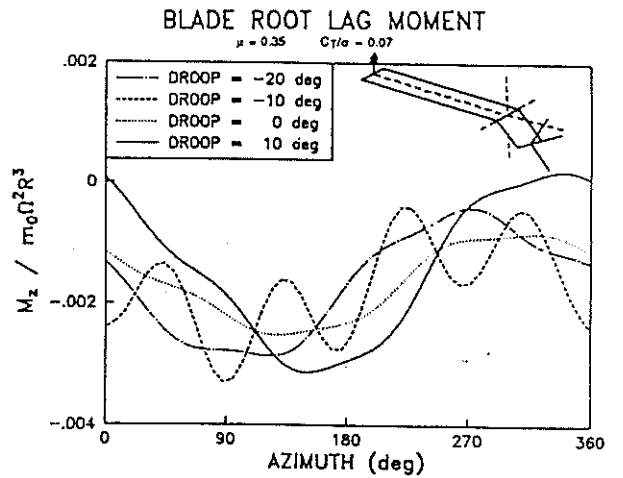
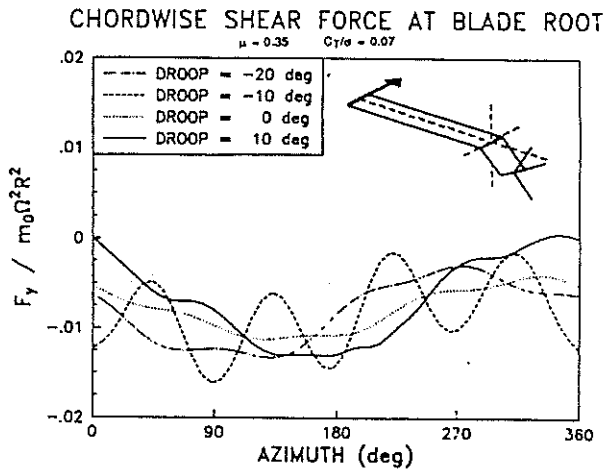
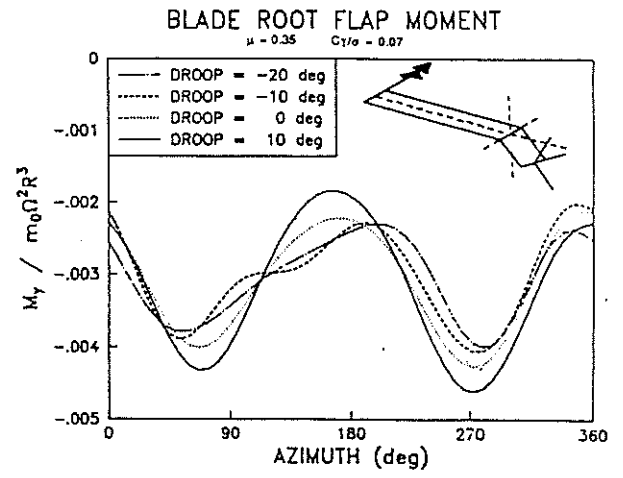
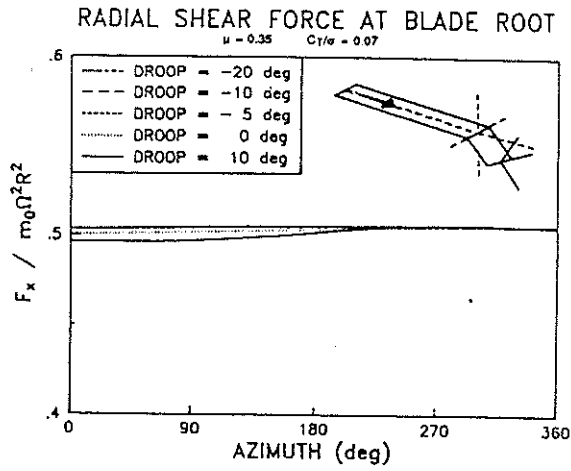


Figure 36



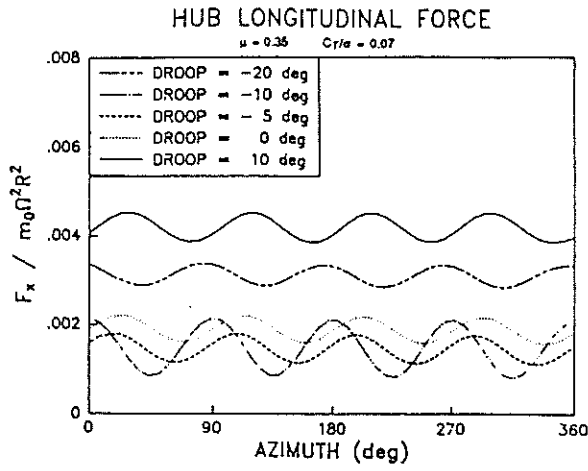


Figure 43

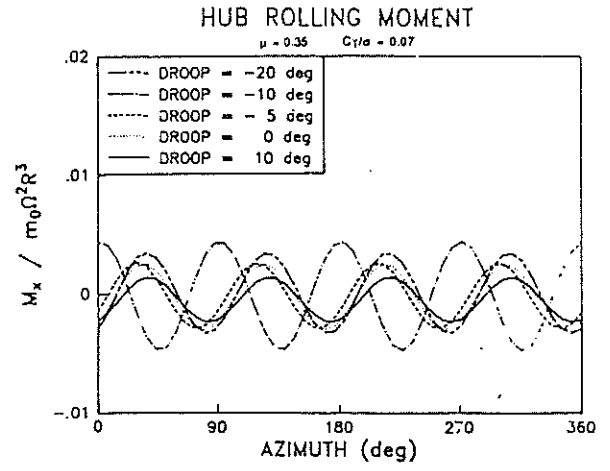


Figure 46

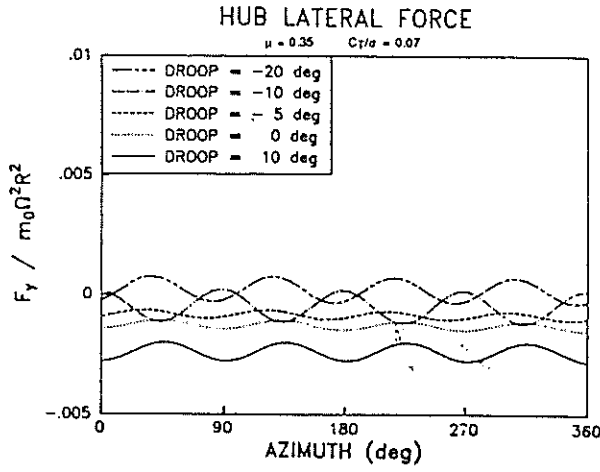


Figure 44

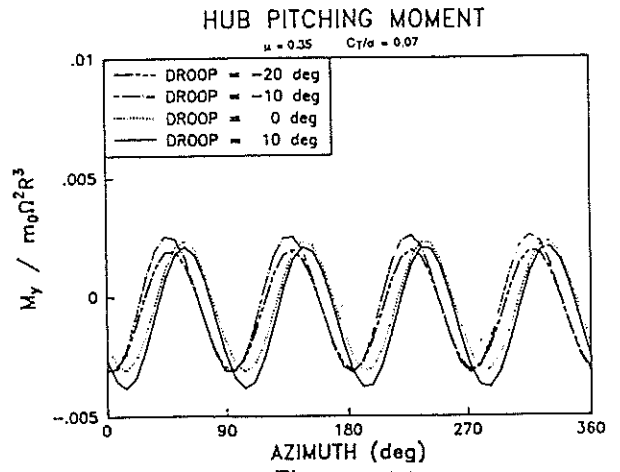


Figure 47

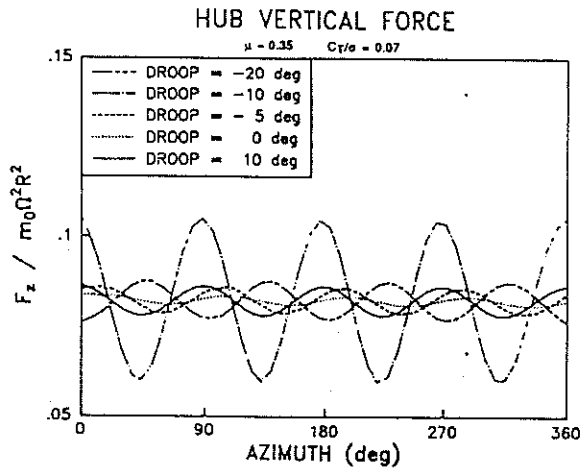


Figure 45

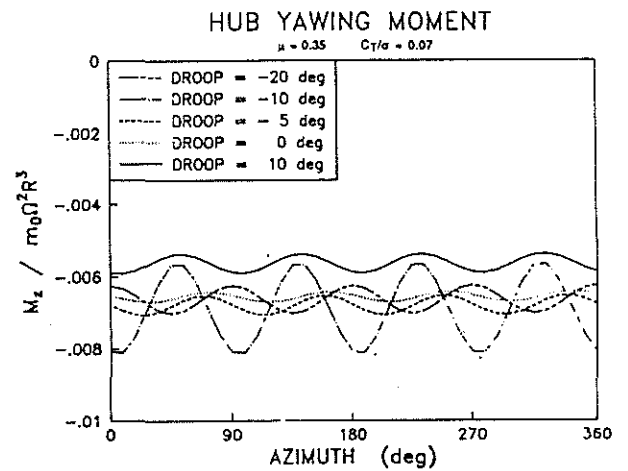


Figure 48

HUB FORCES PEAK-TO-PEAK AMPLITUDES

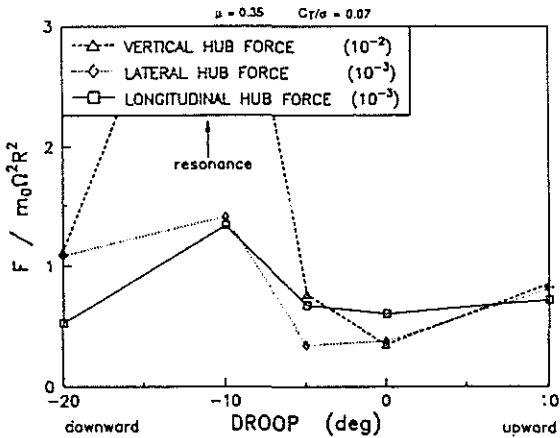


Figure 49

HUB MOMENTS PEAK-TO-PEAK AMPLITUDES

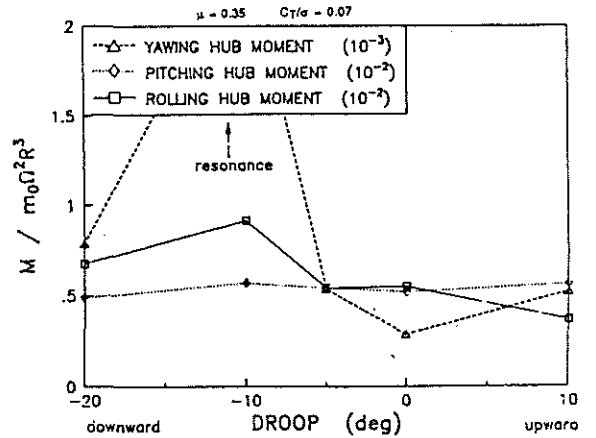


Figure 50